Spatio-temporal Fingerprint Localization for Shipboard Wireless Sensor Networks

Mozi Chen, Kezhong Liu, Jie Ma and Cong Liu

***Abstract*—Location-aware technology has numerous potential applications in safety, living, and services in the shipboard environment. Fingerprint-based methods that use the received signal strength indication (RSSI) to provide high positioning accuracy have been widely adopted for indoor localization. However, RSSI can be severely disturbed by the steel structure and dynamics of the shipboard environment, which prevents it from being implemented in shipboard localization in practice. In this paper, a novel approach, called spatio-temporal fingerprint localization, is proposed. This approach can alleviate the impact of the dynamic shipboard environment and enhance the localization robustness. To adapt to the environmental dynamics, a radio time series is proposed to filter irrelevant noise from location fingerprints. An extraction method called radio spatial features is proposed to identify the highly location related features from redundant RSSI information by using linear discriminant analysis and principal component analysis. Extensive experiments on the passenger ship *Yangtze 2* demonstrate the effectiveness of the proposed algorithm in providing higher accuracy than previous fingerprint-based methods.**

***Index Terms*—Shipboard Environment, Indoor Localization, Fingerprint Localization, Wireless Sensor Network.**

I. Introduction

As location-based services (LBSs) [1] have found increasingly wide and extensive application in different fields, there has been an increasing demand for indoor LBS applications in recent years. As one of the most important means of water transportation, ships such as cruise ships and ferries are important indoor scenes in which hundreds of people will stay for a long duration of a voyage. Real data have shown us how complicated and chaotic the movement of people on a large ship can be [2]. As these ships have large sizes and complex structures, LBS plays an important role for passengers in a wide range of living, safety, and service applications onboard. An accurate built-in localization system and pervasive LBS for passengers can enable them to quickly achieve their goals of all resources in the ship and dramatically reduce the reaction time in an emergency situation.

This work was supported by the National Natural Science Foundation of China (NSFC) under Grant No. 51279151 and 51679182; the Major Project for the Technology Innovation of Hubei Province, China, under Grant No.2017AAA120; and the Fundamental Research Funds for the Central Universities under Grant No. WUT-2017-YB-031.

M. Chen is with the School of Navigation, Wuhan University of Techology, Wuhan 430063, China (e-mail: chenmz@whut.edu.cn).

K. Liu and J. Ma are with the School of Navigation and Hubei Key Laboratory of Inland Shipping Technology, Wuhan University of Techology, Wuhan 430063, China (e-mail: kzliu@whut.edu.cn; majie@whut.edu.cn.

C. Liu is with the Department of Computer Science, The University of Texas at Dallas, Texas 75080, USA (e-mail: cong@utdallas.edu).

* Corresponding author: Jie Ma (majie@whut.edu.cn).

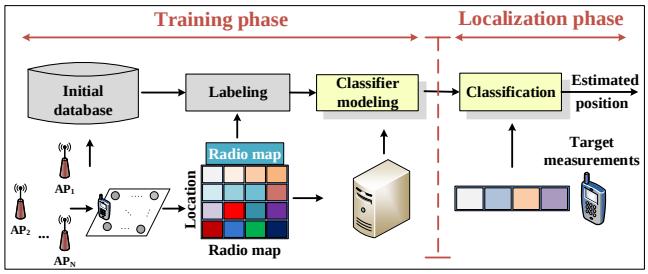

Fig. 1. Architecture of the fingerprinting localization system.

Currently, the Global Positioning System (GPS) [3] is one of the most effective positioning technologies in outdoor environments. However, it has weaknesses, such as being easily shielded by the metal hull and poor signal strength in the shipboard indoor environment. These drawbacks have led to the development of indoor localization techniques based on wireless networks, such as radio frequency identification (RFID) (e.g., LANDMARC [4]), ultra-wideband, ZigBee, and Wi-Fi. Among these technologies, the IEEE 802.15.4/ZigBee standard is assumed to be a good solution for application in the shipboard environment [5]. A self-healing mesh network, which is easy and reliable to deploy on a large scale, can be constructed at low cost [6]. For localization within the ZigBee-based shipboard wireless sensor network, the positioning methods include distance-based (time of arrival and time difference of arrival) [7], [8], [9] and fingerprint-based methods [10], [11] [12]. For the reason of the received signal strength indication (RSSI) can be easily obtained from various hardware devices, RSSI is primarily used in distance-based technologies to estimate distances, even the RSSI can be severely affected by non-line-of-sight (NLOS) scenarios [13]. Unlike distance-based methods, fingerprint-based methods (also referred to as radio mapping), which exploit the existing infrastructure and establish mapping relationships between indoor locations and RSSI signatures without transforming the RSSI values into distance information, have been proposed and are widely adopted for indoor localization [14]. Fig.1 illustrates the fingerprint-based technique. The construction of a radio map is the called offline training phase, and matching is referred to as the online localization phase. Fingerprint-based methods can achieve higher precision in complex indoor environments. However, the RSSI mapping relationships can easily vary as a result of multipath effects in the shipboard environment, which contribute to most of the estimation errors in current localization systems.

In this case, the radio propagation properties and dynamic environment impacts in the shipboard environment have been studied. Extensive experiments have been conducted in a real-world passenger ship to analyze the impacts from both spatial and temporal perspectives. Spatially, signal propagation suffers from a severe multipath effect subject to signal reflection, diffraction, and absorption by steel structures (e.g., water doors and decks) in a real shipboard environment. A signal can propagate through different paths and generate different components, which are combined to reproduce a distorted version of the original signal [15]. Temporally, however, shipboard signal propagation suffers from dynamic changes during the voyage, including transient interference, such as from moving passengers, doors opening and closing, and prolonged changes in terms of the ship speed, temperature, humidity, and weather conditions [16]. As a result, the multipath effect and environmental changes can severely disturb the RSSI measurement and make fingerprints diverge from the radio map, which leads to the deterioration in localization precision. The RSSI impacts in the shipboard environment are summarized as follows:

1) Severe absorption and reflection effects on wireless signals are caused by the steel structures of the ship.
2) Different multipath signals are generated in a narrow structure and multicabin shipboard environment.
3) Shipboard RSSI measurements are severely disturbed by dynamic changes of ship sailing, which generate a time-varying effect.
4) RSSI is sensitive to the movements of passengers and may change significantly in response to human body masking.

To overcome these problems, a novel localization method, called spatio-temporal fingerprint (STF) localization, is proposed to decrease the impact of the shipboard environment and enhance the robustness of the fingerprint localization system. The main idea is to exploit the complementary advantages of spatial features and temporal sequences to solve the above problems. To extract the temporal fingerprint features, a time sequence analysis method called a radio time series (RTS) is proposed to reduce the effect of time variability in RSSI signals and adapt to the dynamic changes of the ship's environment. To further extract the spatial fingerprint features, STF localization computes the difference RSSI between pairs of anchors to reduce the effect of variation among different anchors. A combination of two dimension-reduction methods—linear discriminant analysis (LDA) and principal component analysis (PCA)—is applied to extract the most location-related features called radio spatial features (RSF). With the retention of a sufficient number of location features (namely RSF), irrelevant noise and redundant information are filtered to reduce the computation and alleviate the multipath effect of the shipboard RSSI signals. Based on these spatio-temporal features, a support vector machine (SVM) is utilized to efficiently match the real-time fingerprints with the radio map during the online phase. In the experiments reported in this study, the proposed STF method was applied in a real-world ship to demonstrate that it improves localization accuracy in the shipboard environment compared to the traditional RSSI-based approach. Compared with other traditional fingerprint techniques, the advantages of STF localization are as follows:

1) STF localization achieves good localization in shipboard environments where the traditional fingerprint technique suffers from dramatic performance degradation. The basis of the approach is the computation of the difference RSSI between pairs of anchors and combining this with raw RSSI data to maintain their independence information.
2) STF localization takes complementary advantages of PCA and LDA by combining them in an intelligent manner. Through the combination, STF localization can achieve low computation cost and attract the most location-related features by filtering irrelevant noise and redundant information.
3) STF localization is adaptive to dynamic shipboard environmental changes. Through constructing a time series of localization features, the approach can match the radio map without calibration after the ship begins sailing, thereby achieving more reliable fingerprint features.

The remainder of the paper is organized as follows: in Section 2, theories that have been applied to localization and related works are introduced. Section 3 describes the proposed localization algorithm in detail and Section 4 presents the experimental procedure and results. Finally, the conclusions are drawn in Section 5.

II. PRELIMINARIES

In this section, the preliminary background of radio propagation and the measurements to understand the RSSI dynamics in the shipboard environment are presented. Then, methods to extract fingerprint features to enhance the performance of the fingerprint technique are introduced.

A. Wireless Signal Multipath Effect

According to the Friis model [17], the line-of-sight (LOS) radio propagation path can be described as follows:

$$P_r = |\vec{p}| = \frac{P_t G_t G_r \lambda^2}{(4\pi d)^2}, \tag{1}$$

where P_r is the received signal strength and P_t is the transmitted signal strength, G_t and G_r represent the antenna gains of the transmitter and receiver, respectively, λ is the signal wavelength, and d is the distance of radio propagation. $\vec{p}$ is the radio wave and can be denoted as a vector: $\vec{p} = \{|\vec{p}|, \theta\}$, where $|\vec{p}|$ denotes the signal power and $\theta = 2\pi(d/\lambda)$ is the phase when the transmitter has a phase of zero.

However, many NLOS paths are generated by reflection in narrow shipboard environments as illustrated in Fig. 2. Suppose that there are N paths during propagation. Each of them can only transmit partial energy to the receiver because of the absorption of walls and diverse path lengths. As a result, we can denote the power of the i-th NLOS path as

$$|\vec{p_i}| = \gamma_i \frac{P_t G_t G_r \lambda^2}{(4\pi d_i)^2}, \tag{2}$$

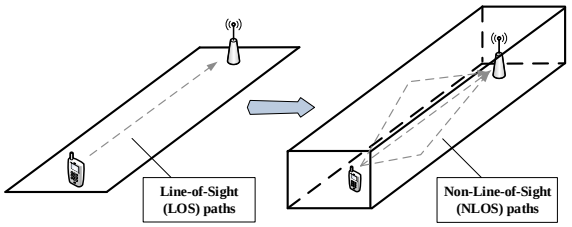

Fig. 2. Illustration of the multipath effect in free space and the shipboard environment.

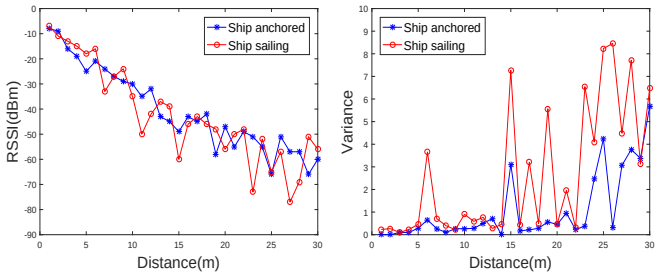

(a) (b)

Fig. 3. RSSI measurements in shipboard environment. (a) Mean RSSI values. (b) Variances of the RSSI values.

where γ_i is the reflection coefficient of the i-th path, which represents the absorption factor of different materials, and d_i is the distance of the NLOS path. Therefore, the received signal strength is the combination of all paths:

$$|\vec{p}| = \left| \sum_{i=1}^{N} \vec{p_i} \right|. \tag{3}$$

The RSSI at distance d under the multipath effect can be further expressed as the combination of LOS path power and NLOS path power:

$$[P_r(d)]_{dB} = 10n \log \left(\gamma \frac{P_t G_t G_r \lambda^2}{(4\pi d)^2} \right) + X_\sigma, \tag{4}$$

where n is an indicator that depends on the propagation environment, and X_σ is a random variable that represents the uncertainty of the multipath effect given by

$$\begin{aligned} X_\sigma = 10n \log \Bigg[& \left(\sum_{i=1}^{N} \gamma_i \frac{P_t G_t G_r \lambda^2}{(4\pi d)^2} \sin(\theta) \right)^2 \\ & + \left(\sum_{i=1}^{N} \gamma_i \frac{P_t G_t G_r \lambda^2}{(4\pi d)^2} \cos(\theta) \right)^2 \Bigg]^{\frac{1}{2}}. \end{aligned} \tag{5}$$

In fact, the multipath parameters N, γ_i, d_i, and θ are unknown and nonconstant. The wireless signals that are transmitted from the transmitter will suffer from reflection because of the influences of walls and decks. The propagation path d_i is randomly extended and the absorption γ is varying according to the number of signal reflections.

B. Time-variant Behavior

A fingerprint-based method collects a radio map of measurement fingerprints and uses a machine learning classifier to determine a target's location using a new fingerprint. However, dynamic changes during ship sailing will generate different noisy signals and disturb the RSSI values severely, which diverge the fingerprints from the constructed map. Shipboard environmental changes include instantaneous interference, such as from doors opening and closing, and long-term changes, such as variations in temperature, humidity, and weather conditions. Path degeneration occurs when the environmental dynamic changes contribute to the variation of the transmission path of the wireless signal. It simultaneously results in fluctuation and mutation of the RSSI.

Fig. 3 shows the changes and fluctuations at different communication distances under sailing and anchoring states. The RSSI continues to show a log-normal behavior with distance. However, there is severe noise in the curve of the sailing state, and there are more severe fluctuations in the RSSI measurement where the transmission distance is large. Meanwhile, the variance of the RSSI measurement in the sailing state is much larger than that in the anchored state at most distances.

C. Fingerprint Feature Extraction Methods

The previous approaches for handling the dynamic environment problem can be classified into two categories: radio map updating and robust feature extraction [16]. Methods of the first category repeat the site survey procedure to collect the RSSI datasets and retrain the fingerprint model. However, this approach is labor intensive and time consuming. Methods of the second category attempt to extract robust fingerprint feature to decrease the impact of the dynamic environment, such as HLF [18], DIFF [19], and SSD [20]. HLF uses the signal strength ratios between pairs of anchor nodes instead of the absolute RSSI. DIFF uses the difference of RSSI values instead of ratios to decrease the computing cost of extracting ratio features. SSD analyses the Cramér–Rao lower bound (CRLB) of localization using the difference RSSI and its performance has been verified theoretically. The difference RSSI shows good performance. The main advantage offered in this paper is using the combination of RSSI and difference RSSI to avoid losing independence information from each anchor.

Because of the extended dimensions, a large number of redundant measurements have to be stored. To overcome this drawback, dimensionality reduction methods are explored to reduce the computational cost while retaining most of the information. For example, in [21], kernel canonical correlation analysis (KCCA) was used to maximize the correlation between the physical location and signal space by matrix transformation. Fang *et al.* explored the possibility of performing PCA to project the RSSI signals into a subspace and improve the positioning accuracy [22]. In PCA, one extracts the most descriptive data but does not consider the underlying RSSI values at different locations. LDA can capture the most discriminative features but has limited effective dimensions and numerical problems. In this paper, both PCA and LDA are utilized to extract fingerprint features.

III. Proposed Algorithm

In this section, novel position fingerprint features, called spatio-temporal features, are proposed to improve the robustness of fingerprint localization. The proposed algorithm employs a three-step approach, which is described in the following subsections.

A. Radio Time Series

To reduce the random variation of the RSSI, an RTS is proposed. In the offline training phase, the localization area is divided into small grids. The total number of grids is denoted as K. To construct a radio map, the target node was used to scan each grid for beacon nodes and extract their MACs and RSSIs with a measurement period of $T = 0.1$ s. The primal fingerprint of the k-th grid can be denoted as

$$F_k = \begin{bmatrix} rssi_1^1 & rssi_2^1 & \cdots & rssi_N^1 \\ rssi_1^2 & rssi_2^2 & \cdots & rssi_N^2 \\ \vdots & \vdots & \ddots & \vdots \\ rssi_1^M & rssi_2^M & \cdots & rssi_N^M \end{bmatrix}, \tag{6}$$

where $rssi_n^m$ is the m-th sample data of corresponding RSSI values of the n-th beacon nodes, which are identified by their MAC address. The total number of samples is M and the number of beacon nodes is N. It should be noted that there is a significant chance of losing signal data from beacon nodes. The RSSI value is automatically completed at -99 dBm, which is the minimum signal strength. In addition, we set the label $y_k \in [1, K]$ to each location grid. Therefore, the primal radio map can be constructed as $X_o = [F_1, F_2, \ldots, F_K]^T$. The label matrix can be denoted as $Y = [y_1, y_2, \ldots, y_K]^T$ to indicate the location information for the radio map.

An RTS is produced by a sliding window, which moves forward with the primal fingerprint F_k and generates new feature series of $\hat{x}$. We define the length of the sliding window as u, which covers a time period of $T \times u$. The time shift of two successive time windows is denoted as T_S. In the RTS extraction procedure, one element $\hat{x}$ from u sets of collected RSSI data (each column of F_k) is extracted during the window. An RTS element $\hat{x}_i$ can be calculated in a sliding window as

$$\hat{x}_n^w = \frac{1}{u}\left(rssi_n^1 + \sum_{i=2}^{u} rssi_n^i e^{-|rssi_n^i - rssi_n^{i-1}|}\right), \tag{7}$$

where w is the index of the sliding window. There is a trade-off among u, T_s, and the speed of the moving target. In the experiment, the walking speed of the experimenter was 1 m/s, and the expected localization accuracy was within 3 m. Hence, the extraction parameters are given as $T_s = 1$ s and $u = 3$. Fig. 4 shows the process of RTS extraction by a sliding window.

B. Radio Spatial Features

Two RSSI values ($rssi_1^m$ and $rssi_2^m$) are measured from the m-th packet of two different beacon nodes at distances d_1 and d_2. According to Eq. 4, we can define

$$rssi_1^m = 10n \log\left(\gamma \frac{P_{t1} G_{t1} G_r \lambda^2}{(4\pi d_1)^2}\right) + X_{\sigma 1} \tag{8}$$

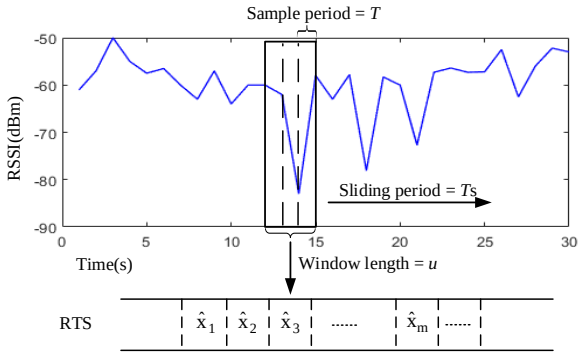

Fig. 4. Extract RTS by a sliding window.

and

$$rssi_2^m = 10n \log\left(\gamma \frac{P_{t2} G_{t2} G_r \lambda^2}{(4\pi d_2)^2}\right) + X_{\sigma 2}. \tag{9}$$

Note that the two factors introduce variation into the measurement: the propagation distance d and multipath effect factor X_σ. If we assume that the beacon nodes have the same transmission power, antenna gain, and wavelength ($P_{t1} = P_{t2}$, $G_{t1} = G_{t2}$ and $\lambda_1 = \lambda_2$), then substituting Eq. 8 and Eq. 9, we obtain

$$rssi_1^m - rssi_2^m = 20n \log\left(\frac{d_2}{d_1}\right) + (X_{\sigma 1} - X_{\sigma 2}). \tag{10}$$

We define the difference RSSI as

$$\hat{x}_{ij}^m = rssi_i^m - rssi_j^m, \quad i, j \in [1, N],\ i < j. \tag{11}$$

Equation 11 shows that the main factor N_σ, which introduces the RSSI variation, is decreased. The difference RSSI is more reliable for the ratios between the distances (d_1 and d_2). Therefore, the RTS values are also combined with the difference RSSI into a fused matrix $\hat{X}_k$ to make use of both advantages instead of F_k. $\hat{X}_k$ can be denoted as

$$\hat{X}_k = \begin{bmatrix} \hat{x}_1^1 & \cdots & \hat{x}_N^1 & \hat{x}_{1,2}^1 & \cdots & \hat{x}_{N-1,N}^1 \\ \hat{x}_1^2 & \cdots & \hat{x}_N^2 & \hat{x}_{1,2}^2 & \cdots & \hat{x}_{N-1,N}^2 \\ \vdots & \cdots & \vdots & \vdots & \cdots & \vdots \\ \hat{x}_1^W & \cdots & \hat{x}_N^W & \hat{x}_{1,2}^W & \cdots & \hat{x}_{N-1,N}^W \end{bmatrix}, \tag{12}$$

where $W = M \times T/T_s$ is the number of windows. Based on the fused feature matrix as the fingerprint, we can obtain the new radio map as $X_d = [\hat{X}_1, \hat{X}_2, \ldots, \hat{X}_K]^T$. The label matrix is also Y.

There are many latent factors in the fused vector that make the RSSI distribution different, which can be seen in Fig.5. Additionally, the dimension of the input fingerprint is changed from (W, N) to (W, $N(N+1)/2$). To reduce the calculation burden and eliminate the impact factors, dimensionality reduction by LDA is considered to extract the most location-related positioning features (RSF) that are more relevant to location labels Y. However, to perform LDA, the input matrix should be invertible. The difference RSSI, which is obtained by linear transformation, is noninvertible and cannot be directly used in LDA. Therefore, PCA is implemented in advance to extract the principal components of position features and eliminate the singularity of the matrix. The main objective of

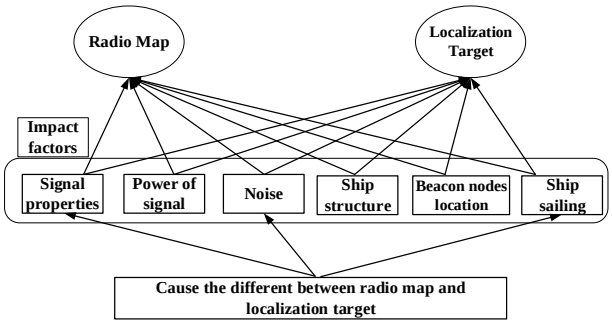

Fig. 5. Factors that impact RSSI measurement in the shipboard environment. Within them, The most location-related features are signal properties, ship structure and beacon nodes locations.

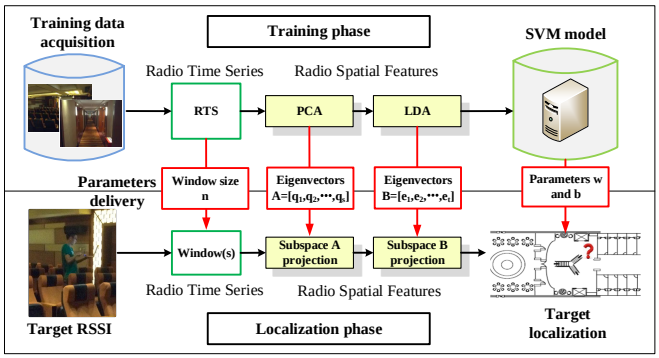

Fig. 6. Flow chart of STF extraction process.

PCA is to find the projection that best represents the dataset. The transformation matrix A is determined by selecting the maximum-variance directions of data as follows:

$$A_{opt} = \arg\max_{A} |A^T S_\Sigma A| \tag{13}$$

where $S_\Sigma \in R^{(N(N+1)/2)*(N(N+1)/2)}$ is the covariance matrix of radio map X_d. It can be calculated as:

$$S_\Sigma = \sum_{s=1}^{S} (\hat{X}_s - \bar{X})^T (\hat{X}_s - \bar{X}) \tag{14}$$

where $\hat{X}_s$ is the s-th row vector of the matrix X_d, $S = K \times W$ is the row number of X_d, and $\bar{X}$ is the global mean of all $\hat{X}_s$. In fact, the solution A_{opt} is a subset of eigenvectors of matrix S_Σ:

$$A_{opt} = [q_1, q_2, \ldots, q_{N(N+1)/2}] \tag{15}$$

where q_i is a $N(N+1)/2$ dimension vector ranked the eigenvalues λ_i in descending order, which quantifies the information that contributes to the i-th eigenvector. Due to the covariance matrix is a positive semi-definite symmetric matrix, the eigenvectors are geometrically orthonormal and statistically uncorrelated. This property guarantees that the generated feature components are uncorrelated to each other. The new feature matrix $X_p \in R^{W*(N(N+1)/2)}$ can be obtained by:

$$X_p = X_d * A_{opt} \tag{16}$$

After eliminating the singularity, LDA can extract the discriminative features of each location fingerprint. The main idea of LDA is to find a projection that will give a large separation between the means of the projected classes (where we define each location grid fingerprint as a class) while giving a small variance within each class. The total within-class variance matrix can be defined as

$$S_W = \sum_{k}^{K} r_k (X_p^k - \bar{X}_p^k)(X_p^k - \bar{X}_p^k)^T \tag{17}$$

where X_p^k is the k-th vector of X_p, $\bar{X}_p^k$ is the global mean of the k-th vector of X_p^k, and r is the discriminant coefficient $r_k = 1$ when x_t belongs to the k-th class; otherwise, $r_k = 0$.

The total between-class scatter matrix of different positions of feature samples can be represented as:

$$S_B = \sum_{k=1}^{K} N_k (X_p^k - \bar{X}_p^t)(X_p^k - \bar{X}_p^k)^T \tag{18}$$

where $N_k = \sum_k^K r_k$. To transform the labeled set of localization features from X_p into a labeled set in subspace X_l, the objective is to find an $(N(N+1)/2) \times t$-dimensional matrix B, which can be obtained by

$$B_{opt} = \arg\max_{B} J(W) = \frac{|B^T S_B B|}{|B^T S_W B|} \tag{19}$$

Maximizing $J(W)$ is the main step of LDA, and the eigenvector of $S_W^{-1} S_B$ with the maximum eigenvalue is the solution. By choosing the first t vectors, the LDA projection matrix B_{opt} can be expressed as:

$$B_{opt} = [e_1, e_2, \ldots, e_t] \tag{20}$$

If projections parameter t is suitably chosen, the RSF X_l can contain large amounts of location-related information and fully removed redundancy. X_l can be obtained by:

$$X_l = X_p * B_{opt} \tag{21}$$

To determine the parameters t of the matrices B, the following mechanism is proposed: t is selected depending on the dimension of the difference RSSI resulting from the goal of breaking the singularity by PCA. The selection of t is determined by the relative proportion of eigenvalues:

$$\frac{\sum_{i=1}^{t} \lambda_i}{\sum_{i=1}^{N(N+1)/2} \lambda_i} \geq \delta, \tag{22}$$

where t is the target RSF dimension. We can set a threshold δ to represent the percentage of the total information. In most cases, δ can be selected as 90% to retain most of the information. The transformations A and B are applied in both the training and online phases.

C. SVM-based Localization Algorithm

To track the positioning problems of search, contrast, and recognition in a radio map, four machine learning classifiers are tested: the K-nearest neighbor (KNN) method [23], logistic regression, SVM, and an artificial neural network (ANN).

Among them, SVM is a supervised learning algorithm that has been used in radio map classifiers. The basic idea of SVM is to map the samples as points in multidimensional space and find an optimal separating hyperplane that maximizes the margin between categories [24]. SVM can use labeled positioning features to train a model that can predict the locations of the new radio features. The radial basis function (RBF) kernel is chosen to handle the problem of different location features being nonlinear. We utilized the open software LIBSVM tools [25] to implement the backend localization algorithm. The whole process of the STF method is shown in Fig. 6.

IV. Experimental Results and Analysis

In this section, the RSSI signals in the shipboard environment are studied and the performance of the STF method is evaluated and analyzed.

A. Environment and Network

In this paper, the shipboard sensor network nodes are designed with Texas Instruments (TI) CC2530 chips, which meet the IEEE 802.15.4/ZigBee protocols and operate in the 2.4 GHz range. Each sensor node is classified as either a receiving or beacon node. Beacon nodes are fixed inside the ship and continuously broadcast radio messages at a rate of 1 package per minute. Receiving nodes are brought by passengers. These nodes collect the RSSI information measured from the beacon nodes and upload it to a server to estimate locations.

The experiments are conducted on the main deck of the inland passenger ship *Yangtze 2*. The main deck area includes a living room (60 m $\times$ 20 m), a dining room (40 m $\times$ 20 m), and a central hall (20 m $\times$ 20 m). These measurements are used during cruises between Chongqing and Yichang (China). A network of nine beacon nodes is deployed on the deck. Eighty reference locations are identified and marked by numbers on the floor. Neighboring reference locations are separated by 200 cm. RSSI at each location is collected for 60 samples.

B. Shipboard Radio Propagation

We performed several experiments to estimate the average losses and propagation parameters in different scenes of the shipboard environment. As introduced in Section II, given fixed transmitter and receiver antenna gains G_t and G_r and fixed transmission power P_t, three parameters would affect the path loss model: the path loss exponent n, the absorption coefficient γ, and the standard deviation σ of the random noise variable X_σ. To study the path loss model of the shipboard environment, several transmitters and receivers were placed at different locations on the main deck at different distances. The RSSI values of different ranges and scenes were collected and a linear regression with a minimum mean square error was utilized to determine the parameters of the path loss model in Eq. 5 for each scene. Table I list the parameters in the four scenes. It also includes the average path loss at $d_0 = 1$ m and the coefficient of correlation r between the measurements for the four scenes.

As we can see, shipboard scenes share different propagation parameters. The correlation coefficients of the four scenes exhibit a bad fit between the measurement results and the path loss models. We can find that the scene with the worst model coefficient is the corridors. This results from the ship architecture that included numerous watertight doors and metal walls. Range-based methods, which transform RSSI values to distance information, are not workable in shipboard environments. Instead, the fingerprint features of RSSI can be more reliable than the range to indicate the location signature.

TABLE I
Path-loss parameters in different shipboard scenarios.

Scenario	n	σ	γ	r	$PL(d_0)$
Corridor	-1.7	8.06	0.81	0.62	-7.7
Central hall	-1.4	7.13	0.85	0.83	-9
Dining hall	-0.9	5.16	0.82	0.80	-8
Passenger cabin	-0.8	4.67	0.83	0.62	-8.9

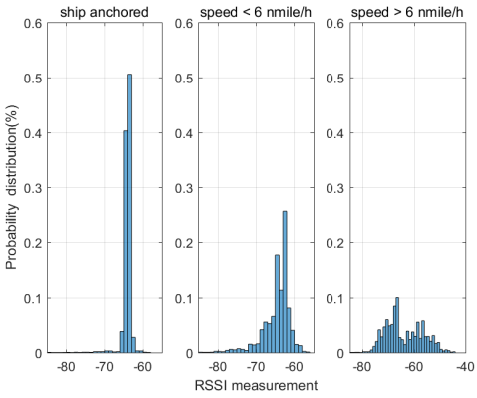

Fig. 7. RSSI distributions in dynamic shipboard environment.

C. RSSI Fluctuations

In Section II, the effect of the ship sailing on shipboard RSSI measurement was simply introduced. Because the ship sailing condition keeps changing and the engines working can affect the quality of wireless communication, it is necessary to conduct the RSSI measurements under different ship sailing states. In this part, the RSSI fluctuations in the shipboard environment under different ship states are tested and analyzed. To measure the ship sailing states, we obtain real-time ship speed data from the ship's internal interface and conduct a point-to-point RSSI measurement test. The receiver is 5 m away from the transmitter and the RSSI values of signal transmission are collected by receiving data packages for three days.

The RSSI probability distributions over time and ship speed are shown in Fig. 7. As can be seen, the RSSI values are basically stable at -65 dBm when the ship is anchored, and they start to fluctuate in the range of 5–15 dBm when the ship speed is 6 nm/h. Once the speed exceeds 6 nm/h, the distribution of RSSI varies from -80 to -40 dBm. The RSSI variance changes as the ship speed increases. The RSSI variances at each speed section are 0.24, 0.45 and 0.92, respectively. The variation of RSSI mean values and standard variances over time and corresponding ship speed are shown in Fig. 8. As can be seen, the mean of the RSSI values during

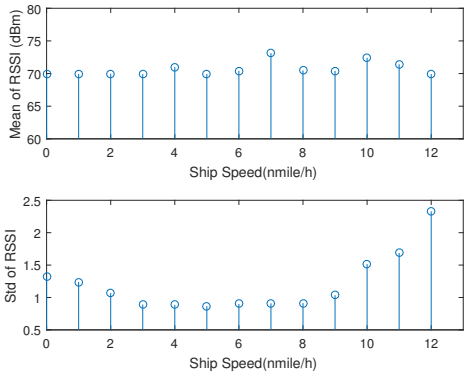

Fig. 8. RSSI distributions in each ship speed.

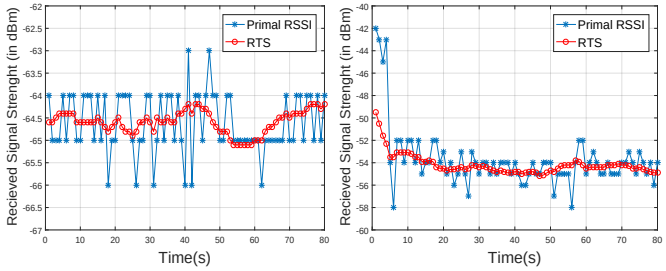

(a) (b)

Fig. 9. RTS visualization. (a) RTS of stationary target. (b) RTS of moving target.

the voyage remained stable when the ship speed was <6 nm/h. Once the speed exceeded 6 nm/h, the RSSI shows a slight change at different speeds. The standard variance of the RSSI is changing follows the ship speed increasing. The RSSI values are basically stable at -65 dBm when the ship is anchored, and they start to fluctuate in the range of 5–15 dBm when the ship sets sail.

D. STF Performance Evaluation

In this part, the performance of STF localization is analyzed. First, RTS and RSF are evaluated and compared with RSSI-based fingerprints. Fig. 9a shows the RSSI and the RTS of a stationary target when the ship is sailing. The RSSI fluctuates in the range of 4 dBm and changes irregularly. The RTS range of variation is reduced to 2 dBm. Fig. 9b shows the performance on the moving target. As can be seen, the RTS extraction can at different ship states. Fig. 10a shows the primal RSSI-based fingerprint distribution in two-dimensional space using PCA for visualization. The points different colored points represent the different RSSI positions. There is a large overlap between points of different colors, which makes the different location features difficult to classify. Fig. 10b shows the RSF distribution in two-dimensional space, which has a better classification character. Here, the primal 9-dimensional RSSI database is used, and a 55-dimensional difference RSSI is obtained. The dimension of the PCA projection is selected to be 50 and that of the LDA is 3.

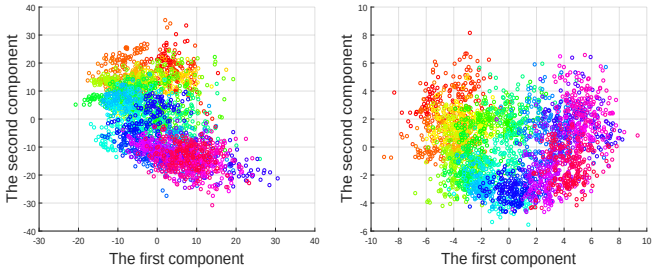

(a) (b)

Fig. 10. Fingerprint visualization. (a) RSSI-based fingerprint. (b) RSF fingerprint.

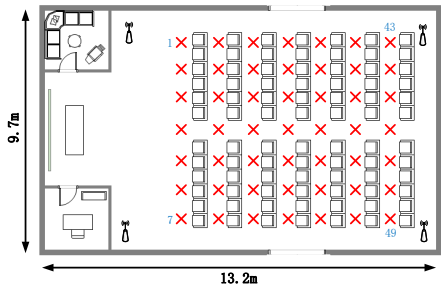

Fig. 11. Lecture theater with node locations.

To evaluate the robustness of STF against environmental changes, a radio map is collected in the lecture theater of the ship, as shown in Fig. 11. The area is approximately 13.2 m $\times$ 9.7 m and is covered by four ZigBee beacon nodes. Forty-nine locations are identified and marked with a red '$\times$.' Neighboring locations are separated from each other by 100 cm. In this experiment, RSSI information of the four beacon nodes is measured 60 times at each reference location when the ship is anchored; this dataset is called the 'anchored dataset'. After the ship sets sail, the RSSI data are collected again and this dataset is called the 'sailing dataset'. The changes in the radio map caused by the dynamic environment are demonstrated in Fig. 12a. Each cell represents a reference location, and dark color means that its RSSI changes enormously. This illustrates that the RSSI-based fingerprint can be significantly affected by the environment and that the impact is irregular. Fig. 12b illustrates that the changes in STF are smaller (paler) under environmental changes and that STF localization has better robustness. The confusion matrices of the RSSI and STF localization are presented in Fig. 13. We can clearly see from Fig. 13b that the localization results are now placed along the diagonals of the matrices, instead of concentrating around a few off-diagonal elements. This suggests that the STF localization is able to extract the stable fingerprint features against the dynamic shipboard environment. From these two figures, we find that our proposed method is more stable under environmental changes than the RSSI fingerprints.

Next, four machine learning classifiers were evaluated: KNN, LR, ANN, and SVM. Table II lists the error of each fingerprinting model, which is trained on anchored STF data and tested on sailing STF data. KNN performs poorly com-

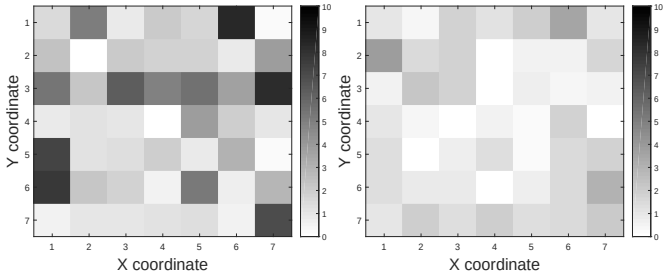

(a) (b)

Fig. 12. Changes in different fingerprints. (a) RSSI. (b) STF.

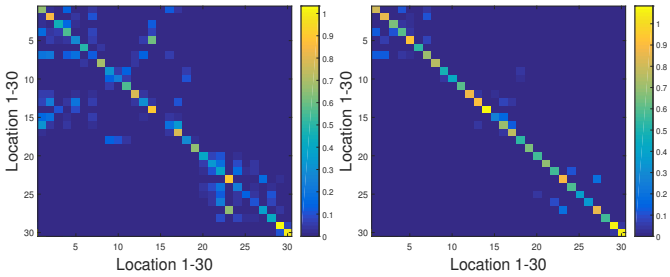

(a) (b)

Fig. 13. Confusion matrices of localization after the environment changes. (a) with RSSI features. (b) with STF features.

TABLE II
ACCURACY CLASSIFICATION FOR FOUR METHODS

Methods	2m	3m	4m	5m	6m	7m
SVM	49.6%	82.4%	96.6%	98.3%	99.1%	99.2%
ANN	50.1%	71.2%	83.3%	90.8%	95.4%	97.3%
LR	42.5%	56.3%	75.2%	84.8%	88.7%	94.3%
KNN	29.3%	49.4%	80.7%	83.5%	85.3%	93.2%

TABLE III
ACCURACY MEASUREMENTS FOR FOUR FEATURES (TRAINING: ANCHOR DATA, TESTING: SAILING DATA)

Features	2m	3m	4m	5m	Average (m)
STF	49.6%	82.4%	96.6%	97.3%	2.92
SSD	38.4%	71.3%	89.3%	96.6%	3.30
HLF	36.4%	60.2%	78.1%	89.5%	3.27
RSSI	9.8%	24.4%	45.3%	71.2%	4.50

pared with the other methods, even using the RSF radio map. The accuracy of KNN only reaches 80% if the separation is >4 m, while SVM can achieve the same accuracy at a separation of 3 m. Increasing K cannot improve the accuracy of KNN. LR also performs relatively poorly. Its accuracy is higher than that of KNN when the separation is <3 m and becomes similar after the separation increases to >4 m. At a separation of 3 m, the recognition accuracy is 56.3%, whereas SVM achieves 82.4%. The adopted ANN contains an input layer, a hidden layer (a logistic function with 100 neurons), and an output layer. The result indicates that the SVM-based positioning algorithm still provides higher accuracy than the ANN-based algorithm.

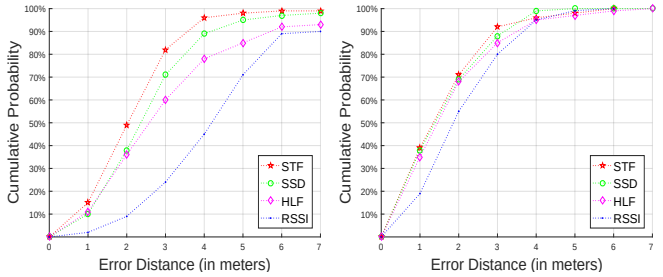

(a) (b)

Fig. 14. Localization error. (a) Environmental change. (b) Environmental stability.

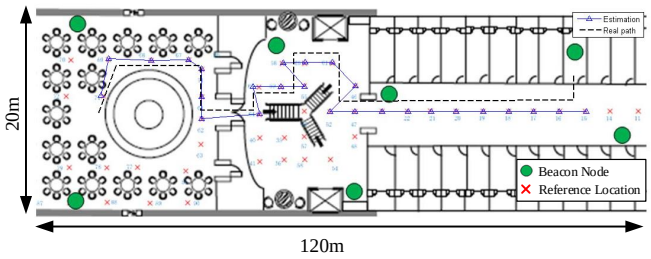

Fig. 15. Trajectory of a subject walking along the deck.

E. Location Estimation Accuracy

In this section, the localization accuracy of STF localization is evaluated by cross-validation. Here, cross-validation refers to training the model using the 'anchored dataset' and testing the model using the 'sailing dataset.' SVM is adopted to model the radio map in this experiment. Fig. 14a displays the cumulative positioning errors of four features—RSSI, SSD, HLF and STF—without cross-validation. These models are both trained and tested on the anchored dataset. These results show that the performance of the proposed STF localization is similar to that of RSSI when the ship remains anchored. Fig. 14b compares the positioning results using cross-validation, in which the training data are selected from the anchored dataset and the testing data are selected from the sailing dataset. Here, STF localization achieves an accuracy of 82.85% at a separation of 3 m, while SSD, HLF, and RSSI obtain accuracies of 71.31%, 60.52%, and 24.83%, respectively. The accuracies of fingerprinting are numerically reported in Table III, including a 2–5 m separation and the mean distance error. The result shows that the accuracy of STF localization is 2.92 m, whereas that of the RSSI-based fingerprint is 4.50 m.

Finally, the robustness of trajectory estimation by STF localization is verified. An experimenter walked through these reference points with a receiving node. The result is shown in Fig. 15. Over a range, the STF localization method can locate targets within 2.5 m of their actual positions with 90% accuracy, which is acceptable for most LBS applications. The average tracking latency of this system can reach 0.01 s, which is significantly shorter than that of previous localization methods.

V. Conclusion

A key challenge for shipboard fingerprint localization is how to handle the problem of dynamic environmental change. This paper proposes an enhanced localization method, spatio-temporal fingerprint localization, to defend against such variation effects. The main idea is to alleviate the effects of two phenomena on wireless signals in the shipboard environment: signal multipath and ship motion. An extraction method using radio spatial features is proposed to extract the highly location related features, which can reduce the interference of the signal multipath in the shipboard environment. Additionally, a radio time series is proposed to filter irrelevant noise to reduce the effects of ship motion. The experimental results indicate that the localization error is 2.92 m. This method significantly improves the results compared with those from traditional fingerprint localization methods.

References

[1] A. Dey, J. Hightower, E. de Lara, and N. Davies, "Location-based services," *IEEE Pervasive Computing*, vol. 9, no. 1, pp. 11–12, 2010.

[2] C. Casareale, G. Bernardini, A. Bartolucci, F. Marincioni, and M. DOrazio, "Cruise ships like buildings: Wayfinding solutions to improve emergency evacuation," in *Building Simulation*, vol. 10, no. 6. Springer, 2017, pp. 989–1003.

[3] P. Misra, B. P. Burke, and M. M. Pratt, "GPS performance in navigation," *Proceedings of the IEEE*, vol. 87, no. 1, pp. 65–85, 1999.

[4] L. Ni and a.P. Patil, "LANDMARC: indoor location sensing using active RFID," *Proceedings of the First IEEE International Conference on Pervasive Computing and Communications, 2003. (PerCom 2003).*, pp. 407–415, 2003.

[5] H. Kdouh, G. Zaharia, C. Brousseau, G. El Zein, and G. Grunfelder, "ZigBee-based sensor network for shipboard environments," *ISSCS 2011 - International Symposium on Signals, Circuits and Systems, Proceedings*, pp. 229–232, 2011.

[6] K. Liu, T. Yang, J. Ma, and Z. Cheng, "Fault-Tolerant Event Detection in Wireless Sensor Networks using Evidence Theory," *KSII Transaction on Internet and Infomation Systems*, vol. 9, no. 10, pp. 3965–3982, 2015.

[7] J. Shen, A. F. Molisch, and J. Salmi, "Accurate Passive Location Estimation Using TOA Measurements," *IEEE Transactions on Communications*, vol. 11, no. 6, pp. 2182–2192, 2012.

[8] H. J. Shao, X. P. Zhang, and Z. Wang, "Efficient closed-form algorithms for AOA based self-localization of sensor nodes using auxiliary variables," *IEEE Transactions on Signal Processing*, vol. 62, no. 10, pp. 2580–2594, 2014.

[9] F. Wen and C. Liang, "Fine-grained indoor localization using single access point with multiple antennas," *IEEE Sensors Journal*, vol. 15, no. 3, pp. 1538–1544, 2015.

[10] A. Arya, P. Godlewski, M. Campedel, and G. Du Chene, "Radio database compression for accurate energy-efficient localization in fingerprinting systems," *IEEE Transactions on Knowledge and Data Engineering*, vol. 25, no. 6, pp. 1368–1379, 2013.

[11] Q. Jiang, Y. Ma, K. Liu, and Z. Dou, "A Probabilistic Radio Map Construction Scheme for Crowdsourcing-Based Fingerprinting Localization," *IEEE Sensors Journal*, vol. 16, no. 10, pp. 3764–3774, 2016.

[12] X. Chen, C. Ma, M. Allegue, and X. Liu, "Taming the inconsistency of Wi-Fi fingerprints for device-free passive indoor localization," *Proceedings - IEEE INFOCOM*, 2017.

[13] Y. Shi, "Improving the performance of RSS detection using wireless open-source platforms," *2015 Texas Symposium on Wireless and Microwave Circuits and Systems, WMCS 2015*, 2015.

[14] M. Brunato and R. Battiti, "Statistical learning theory for location fingerprinting in wireless LANs," *Computer Networks*, vol. 47, no. 6, pp. 825–845, 2005.

[15] X. Guo, D. Zhang, K. Wu, and L. M. Ni, "MODLoc: Localizing multiple objects in dynamic indoor environment," *IEEE Transactions on Parallel and Distributed Systems*, vol. 25, no. 11, pp. 2969–2980, 2014.

[16] B. Mager, P. Lundrigan, and N. Patwari, "Fingerprint-based device-free localization performance in changing environments," *IEEE Journal on Selected Areas in Communications*, vol. 33, no. 11, pp. 2429–2438, 2015.

[17] A. Goldsmith, *Wireless communications*. Cambridge university press, 2005.

[18] M. B. Kjærgaard, "Indoor location fingerprinting with heterogeneous clients," *Pervasive and Mobile Computing*, vol. 7, no. 1, pp. 31–43, 2011.

[19] F. Dong, Y. Chen, J. Liu, Q. Ning, and S. Piao, "A calibration-free localization solution for handling signal strength variance," *Lecture Notes in Computer Science*, vol. 5801 LNCS, pp. 79–90, 2009.

[20] A. K. M. M. Hossain and W. S. Soh, "Cramér-Rao bound analysis of localization using signal strength difference as location fingerprint," *Proceedings - IEEE INFOCOM*, no. 1, 2010.

[21] J. J. Pan, J. T. Kwok, Q. Yang, and Y. Chen, "Multidimensional vector regression for accurate and low-cost location estimation in pervasive computing," *IEEE Transactions on Knowledge and Data Engineering*, vol. 18, no. 9, pp. 1181–1193, 2006.

[22] S. H. Fang, T. N. Lin, and P. Lin, "Location fingerprinting in a decorrelated space," *IEEE Transactions on Knowledge and Data Engineering*, vol. 20, no. 5, pp. 685–691, 2008.

[23] A. K. M. Mahtab Hossain, Y. Jin, W. S. Soh, and H. N. Van, "SSD: A robust RF location fingerprint addressing mobile devices' heterogeneity," *IEEE Transactions on Mobile Computing*, vol. 12, no. 1, pp. 65–77, 2013.

[24] E. Alpaydin, *Introduction to machine learning*. MIT press, 2014.

[25] C.-C. Chang and C.-J. Lin, "Libsvm: a library for support vector machines," *ACM transactions on intelligent systems and technology (TIST)*, vol. 2, no. 3, p. 27, 2011.

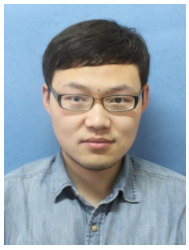

Mozi Chen received the B.S. degree in electric engineering from the Hubei University of Technology, China, in 2013, and the M.S. degree in navigation engineering from the Wuhan University of Technology (WUT), China, in 2016. He is currently a Ph.D. student in WUT. His research interests focused on wireless sensor networks and indoor localization.

Kezhong Liu received the B.S. and M.S. degrees in marine navigation from the Wuhan University of Technology(WUT), Wuhan, China, in 1998 and 2001, respectively. He received the Ph.D. degree in communication and information engineering from the Huazhong University of Science and Techonogy, Wuhan, China, in 2006. He is currently a professor with School of Navigation, WUT. His active research interest include indoor localization technology and data mining for ship navigation.

Jie Ma received the Ph.D. degree in computer science from the Huazhong University of Science and Technology, China, in 2010. He is currently an associate professor in the School of Navigation at the Wuhan University of Technology. His research includes networked sensing systems and data driven intelligent transportation systems, supported by National Natural Science Foundation of China. He has published over 20 journal and conference papers in the related fields.

Cong Liu received the Ph.D. degree in computer science from the University of North Carolina at Chapel Hill, in Jul. 2013. He is an assistant professor in the Department of Computer Science, University of Texas at Dallas. His research interests include real-time systems and GPGPU. He has published more than 30 papers in premier conferences and journals. He received the Best Paper Award at the 30th IEEE RTSS and the 17th RTCSA. He is a member of the IEEE.